

See discussions, stats, and author profiles for this publication at: <https://www.researchgate.net/publication/345769170>

In-route inductive versus stationary conductive charging for shared automated electric vehicles: A university shuttle service

Article in *Applied Energy* · January 2021

DOI: 10.1016/j.apenergy.2020.116132

CITATIONS

0

READS

94

3 authors, including:



Ahmed A. S. Mohamed

National Renewable Energy Laboratory

74 PUBLICATIONS 613 CITATIONS

[SEE PROFILE](#)

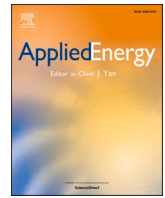
Some of the authors of this publication are also working on these related projects:



System design and Feasibility Analysis of Wireless Charging for LD/MD/HD EVs [View project](#)



EMI in DC-DC converter PCB design [View project](#)



In-route inductive versus stationary conductive charging for shared automated electric vehicles: A university shuttle service

Ahmed A.S. Mohamed^{*}, Eric Wood, Andrew Meintz

Center for Integrated Mobility Sciences, National Renewable Energy Laboratory (NREL), Golden, CO, USA

HIGHLIGHTS

- Techno-economic analysis of in-route inductive charging for automated shuttles.
- Cost models for in-route inductive charger, DC fast charger, and Level 2 charger.
- Powertrain model for automated electric shuttles using real-world collected data.
- Quasi-dynamic inductive chargers at designated stops enable continuous operation.
- In-route inductive chargers are cost-competitive to stationary fast chargers.

ARTICLE INFO

Keywords:

Automated electric shuttles
In-route inductive charging
Optimization
System planning
Inductive power transfer (IPT)

ABSTRACT

In-route inductive charging technology, as applied to automated electric vehicles, can help realize a fully automated system of both vehicles and chargers. This study presents a planning optimization analysis for fixed-route automated shuttles supported by in-route inductive charging technology. A techno-economic feasibility of inductive charging was assessed in comparison with stationary charging, including Level 2 AC chargers, and DC fast chargers (DCFCs). This analysis considered both present-day and future vehicle operations and overall system costs. A real project with two circulator Navya Arma shared automated electric vehicles (SAEVs) at the University of Michigan was investigated using real-world collected energy and travel data. The outcomes show that the proper design of quasi-dynamic inductive chargers at designated stops allows SAEVs to realize unlimited driving range and be cost-competitive to DCFC technology. Considering present-day costs and vehicles, low-speed SAEVs can realize charge-sustaining operation at a minimum cost either by implementing a 50-kW inductive charger at two stops with one segment per position and a 29-kWh onboard battery, or by installing a 100-kW inductive charger at one stop with one segment per position and a 28-kWh onboard battery. Considering future costs and vehicles, either a 40-kW charger at one stop with a 29-kWh battery or a 50-kW charger at the north stop with a 14-kWh battery would enable charge-sustaining operation. In addition, quasi-dynamic inductive solution can reduce the onboard battery by about 15% while providing unlimited driving range, but stationary scenarios require about 112% additional battery capacity to support a 12-h driving range.

1. Introduction

Ground transportation plays a vital role in people's lives. Individuals depend on transportation not only to get to work but also to shop, socialize, and access health care, among other goals. The current ground transportation system experiences several challenges related to safety, cost, and environmental impact: it imposes large costs, loses time in traffic congestion, causes deaths and injuries from crashes, depends on imported petroleum, and releases greenhouse gas emissions and other

forms of pollution [1,2]. Recently, three revolutions in the transportation sector have emerged: electrification, automation, and shared mobility [3]. These revolutions are driven by shared automated electric vehicles (SAEVs) technology. Large-scale deployment of SAEVs has the potential to significantly shape the current transportation system and make our urban mobility safer, less expensive, and more efficient, convenient, and environmentally friendly [4,5]. However, one of the main limitations of electric vehicles (EVs) in general, and SAEVs in particular, is the limited driving range—associated with the limited battery capacity and high energy consumption due to the low-speed

^{*} Corresponding author at: Center for Integrated Mobility Sciences, National Renewable Energy Laboratory (NREL) Golden, CO 80401-3305 United States.
E-mail address: Ahmed.Mohamed@nrel.gov (A.A.S. Mohamed).

Nomenclature**Abbreviations**

AC	Alternating Current
C-rate	Charging Rate
DC	Direct Current
DCFC	Direct Current Fast Chargers
DIPT	Dynamic Inductive Power Transfer
DOE	Department Of Energy
EV	Electric Vehicle
EVSE	Electric Vehicle Supply Equipment
FASTSim	Future Automotive Systems Technology Simulator
GA	Genetic Algorithm
GPS	Global Positioning System
ICE	Internal Combustion Engine
IPT	Inductive Power Transfer
L2	Level 2
N	North
NLMI	Nonlinear Mixed-Integer
OLEV	On-Line Electric Vehicle
QDIPT	Quasi-Dynamic Inductive Power Transfer
S	South
SAEV	Shared Automated Electric Vehicle
SOC	State-Of-Charge
U-M	University Of Michigan
VTO	Vehicles Technologies Office
Δ SOC	Operating State-Of-Charge Window

Variables

ϵ	upper limit of $ SOC_f - SOC_i $
c_{VA}	vehicle assembly cost coefficient
c_b	onboard battery module cost coefficient
C_{r_DCFC}	Total cost of DCFC
N_{DCFC}	number of charging ports
c_{DCFC}	DCFC unit cost coefficient
$c_{DCFC,i}$	DCFC installation cost coefficient
C_{r_L2}	total cost of L2 charger
N_{L2}	number of charging ports
SOC_f	final battery SOC
SOC_i	initial battery SOC
a, b	battery cost coefficients
SOC_{max}	maximum battery SOC

P_E	battery power due to vehicle's dynamics
P_{drag}	drag power
P_{acc}	acceleration power
P_{asc}	ascent power
P_{aux}	auxiliary load power
D_{air}	air density
C_{drag}	drag coefficient
A_f	frontal area
ν	driving speed
τ	current time step
G	gravity
g	road grade
M_v	total vehicle mass
M_{base}	vehicle base mass
D_b	battery density
Q_b	battery capacity
N_{IPT}	number and locations of inductive chargers
N_s	number of track segments at each position
P_c	charging power
P_{bat}	total battery power
P_{IPT}	battery power due to IPT system
$C_{r,IPT}$	road components cost
$C_{v,IPT}$	vehicle components cost
N_L	number of electrified lanes per road
N_{pad}	number of inductive pads per vehicle
N_{SAEV}	number of SAEVs supported by IPT system
x_k	optimization variable k
x_k^L	lower limit of optimization variable k
SOC_{min}	minimum battery SOC
x_k^U	upper limit of optimization variable k
c_r	road construction cost coefficient
c_{em}	road electronics and materials cost coefficient
c_g	grid connectivity cost coefficient
$c_{i,IPT}$	transmitter installation cost coefficient
c_{L2}	L2 charger unit cost coefficient
$c_{L2,i}$	installation cost coefficient
c_{OBC}	onboard charger cost coefficient
$C_{r,lim}$	upper limit of Charging rate
A	lower Limit of minimum battery SOC
B	upper Limit of maximum battery SOC

operation and the additional accessories for automation (e.g., sensors, cameras, lasers, and lidar) [4,6]. In addition, these accessories, along with the large onboard battery, increase the vehicle price compared to the conventional internal combustion engine (ICE) vehicle. Thus, it is crucial to find a solution that both overcomes the range issue, allowing SAEVs to run continuously for over 12 h, as well as brings down the vehicle costs (capital and operating) to be affordable for individuals and commercial fleet companies. One way is to mount a large battery on the vehicle and a stationary overnight charging capability [7]. However, this path leads to an expensive vehicle, due to the large onboard battery, with high operating costs due to the extra size and mass. Furthermore, installing a large onboard battery does not eliminate the range anxiety problem since the vehicles still must stop for recharging. The other pathway is to install in-route charging capability such that SAEVs can be charged during transient stops (quasi-dynamic charging) or while moving (dynamic charging) [8]. This path has the potential to dramatically extend vehicle's driving range (essentially indefinitely), and theoretically eliminate recharge downtime through realizing continuous operation. In addition, it enables the use of a smaller onboard battery, which helps to reduce the vehicle's capital and operating costs [9]. A

good candidate for in-route charging is inductive power transfer (IPT) technology, which allows an EV to charge its energy storage system without physical connection. This technology, applied to SAEVs, could be an ideal fit for realizing a fully automated vehicle and charger. Furthermore, inductive chargers are safer in harsh environments, reliable during extreme weather conditions, flexible (can be installed at designated stops and/or on the road), and interoperable so that the installed system can be used by different vehicles [10–12]. The key challenge of in-route inductive charging technology is the high initial investment for road construction, constituent materials (ferrites, wires, shields, etc.), power converters, grid connectivity, and installation work. However, this high cost can be significantly reduced by realizing the proper system design for the charging infrastructure (number and locations of inductive chargers, power level, and transmitter length). In addition, it can be at least partially balanced by the reduced vehicle cost due to enabling a smaller onboard battery, smaller fleet size (as each vehicle can run for a longer time), and the reduced operating costs [4]. Existing literature includes abundant studies on inductive charging systems, which cover components' design, modeling, control, optimization, prototyping, and testing [8,13–20]. In addition, there are several

ongoing projects to demonstrate the feasibility and reliability of in-route inductive charging technology for different transportation modes, such as public buses [21], fixed-route shuttles [20,22], taxis [23,24], personal vehicles, and trucks on highways [25]. Most of these projects focus on system development, hardware implementation, operation, and safety, but lack for system planning analysis that enables a cost-competitive technology. Planning of this technology is crucial to reduce the overall system cost, which is highly dependent on the system length, placement, and rated power, in addition to the coupled relationship between these parameters and vehicle's cost due to the possibility to install a smaller onboard battery [26]. Few studies have explored in-route inductive charger from the system level design and planning prospective. In [27], the system characteristics of the On-Line Electric Vehicle (OLEV) were investigated for shared shuttle service. That work showed promising results for the specific OLEV bus-case, but it is not fully applicable for SAEV scenarios because it assumed a regulated speed profile and fixed charging power, neglected the vehicle's dynamics, and considered a fixed power block model for the inductive charger and discarded important features, such as charger design, dimensions, and misalignment. In [28], a cost-of-ownership-based optimization analysis for light-duty vehicles with dynamic inductive charging was presented. A system-level optimization model for the power level and road coverage of dynamic chargers on highways considering fixed speed and battery capacity was presented in [29]. In [4,9,30], a design optimization problem for an inductive charging system serving shared automated vehicles in an automated mobility district was presented. The authors considered simulated road networks and assumed linear relationships among optimization variables and objectives. None of the above-mentioned work considered actual representation for SAEV or real-world travel data. In addition, they focus on inductive charging technology without comparing it with other equivalent technologies.

Different from these studies, this paper explores the different options for extending the driving range of SAEVs, considering in-route inductive and stationary conductive charging. The key contributions are:

- Develops and validates a powertrain model for SAEVs using real-world collected energy data,
- Develops an inductive charger power model, considering locations, power level, and misalignments, and links it with the vehicle powertrain model and an automatic search algorithm to form a system planning optimization tool,
- Develops cost models for the SAEV system, considering EV supply equipment (EVSE) (in-route inductive chargers, DC fast chargers (DCFC), and Level 2 (L2) AC chargers) and vehicle components,
- Formulates and solves system design optimization problems for in-route inductive charging for two Navya Arma SAEVs running at the University of Michigan (U-M), Ann Arbor considering present-day and future operation, and
- Presents a comparative study among the different equivalent charging technologies in terms of cost and performance.

The rest of the paper is organized as follows: Section 2 describes the project under consideration and data used; Section 3.1 presents analytical modeling for the SAEV with inductive charging; Section 3 introduces system planning optimization problem formulation; Section 5 presents the outcomes from the study and compares between different charging solutions; and finally Section 6 concludes the study and summarizes the findings.

2. Description of case study

2.1. A. Navya Arma circulator shuttle service

In June 2018, Mcity, a public-private partnership at U-M, launched the first automated shuttle project in the United States. Two Navya Arma automated electric shuttles were deployed to transport students, faculty,

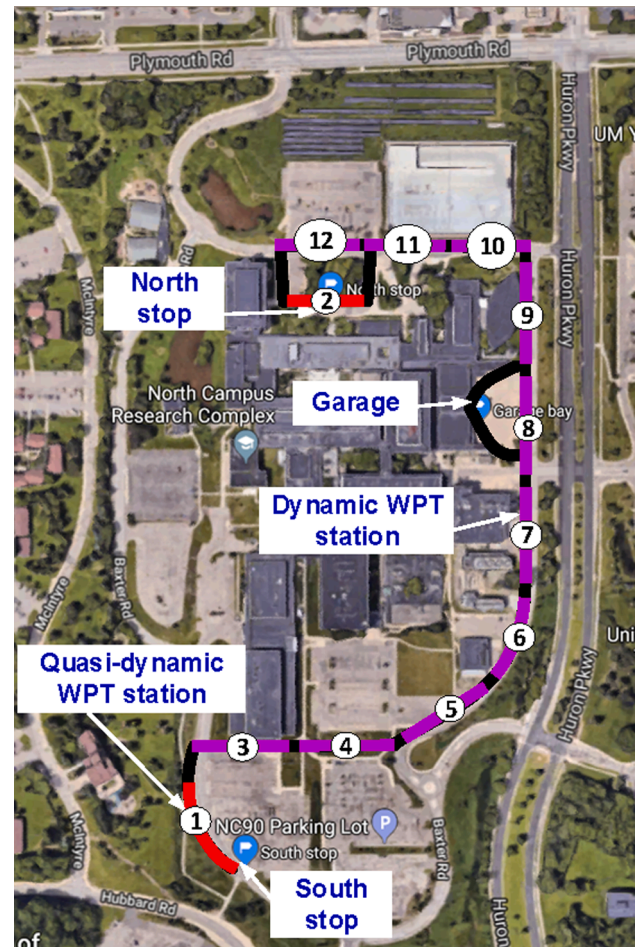


Fig. 1. Route of Navya Arma SAEVs at U-M from Google Maps.

Table 1
3-days of real-world collected GPS travel and energy data.

Vehicle	Navya Arma1			Navya Arma2		
	16	17	19	16	17	19
Avg. speed (mph)	2.938	2.67	3.041	1.737	3.028	3.133
Distance (miles)	17.14	16.54	19.9	10.43	19.47	19.55
AC energy (kWh)	37.50	29.36	30.76	38.03	30.75	38.11
AC kWh/mile	2.19	1.78	1.55	3.65	1.58	1.95

and staff at the U-M north campus [31]. The shuttles circulate in a fixed route (~1 mile) with two designated stops—south (S) and north (N)—for loading and unloading passengers, as indicated in Fig. 1. Arma shuttles are supported with 33-kWh onboard batteries and L2 onboard plugin chargers at the garage area.

2.2. Collected real-world data

One of the goals of the Navya shuttles project is to collect data from the vehicles, chargers, and users to understand vehicle performance, roadway interactions, and passenger attitudes. Among the collected information is global positioning system (GPS) vehicle drive data (e.g., speed, latitude, longitude, and road grade) and charging energy data (AC kWh). Three days of data on July 16, 17, and 19, 2018 were leveraged from the project to be considered for charging infrastructure planning and optimization, as indicated in Table 1 and Fig. 2.

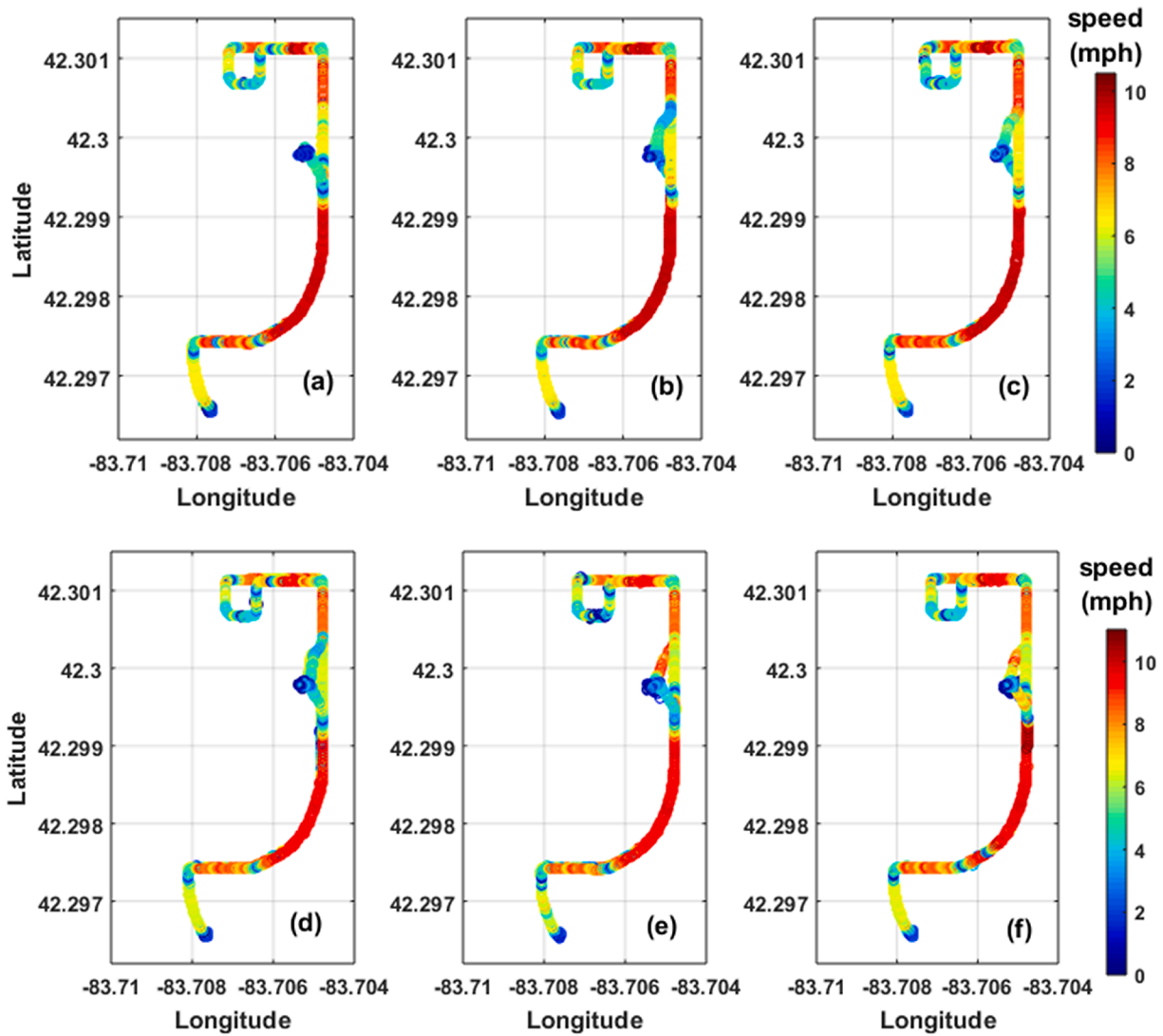


Fig. 2. Real-world collected GPS data from Navya shuttles: (a) Arma1 on July 16, (b) Arma1 on July 17, (c) Arma1 on July 19, (d) Arma2 on July 16, (e) Arma2 on July 17, and (f) Arma2 on July 19.

3. Analytical models of system components

A powertrain model for the vehicle and a power model for the charger are developed and integrated to predict the total battery power, energy, and state-of-charge (SOC) profiles, considering vehicle dynamics (driving and regenerative braking) and charging events.

3.1. Navya Arma powertrain model

A powertrain and energy estimation model for Arma SAEV is developed based on the open-source Future Automotive Systems

Technology Simulator (FASTSim) [32]. The model receives time series of driving speed (with 1-Hz resolution) and calculates the battery electric power (P_E [kW]) due to driving and regenerative braking. The power calculation is performed at each time step, considering: (1) drag power (P_{drag} [kW]), which is required to overcome drag force as described in Eq. (1); (2) acceleration power (P_{acc} [kW]), which defines the power needed to accelerate the vehicle from a current speed to a target speed, as in Eq. (2); (3) ascent power (P_{asc} [kW]), which denotes the excess power for a vehicle to overcome the gravity to drive on roads with inclines, as in Eqs. (3); and (4) auxiliary load power (P_{aux} [kW]), which is needed to keep the vehicle operating and supply sensors, cameras, and computer processors, which is discussed in the next section.

$$P_{drag}(\tau) = 6.25 \times 10^{-5} D_{air} C_{drag} A_f [\nu(\tau - 1) + \nu(\tau)]^3 \quad (1)$$

$$P_{acc}(\tau) = 5 \times 10^{-4} \left(\frac{M_v}{\tau} \right) [\nu(\tau)^2 - \nu(\tau - 1)^2] \quad (2)$$

$$P_{asc}(\tau) = 5 \times 10^{-4} GM_v \sin(\tan^{-1}[g(\tau)]) [\nu(\tau - 1) + \nu(\tau)] \quad (3)$$

$$P_E(\tau) = P_{drag}(\tau) + P_{acc}(\tau) + P_{asc}(\tau) + P_{aux}(\tau) \quad (4)$$

where D_{air} is the air density (1.225 kg/m^3), C_{drag} is the drag coefficient,

Table 2

Parameters of Navya Arma automated electric vehicle.

Parameter	Value
Current battery capacity	33 kWh
Vehicle base mass (M_{base})	3120 kg
Battery density (D_b)	0.125
Drag coefficient (C_{drag})	0.6
Frontal area (A_f)	5.5915 m ²
Wheel radius	0.34544 m
Wheelbase	2.8 m

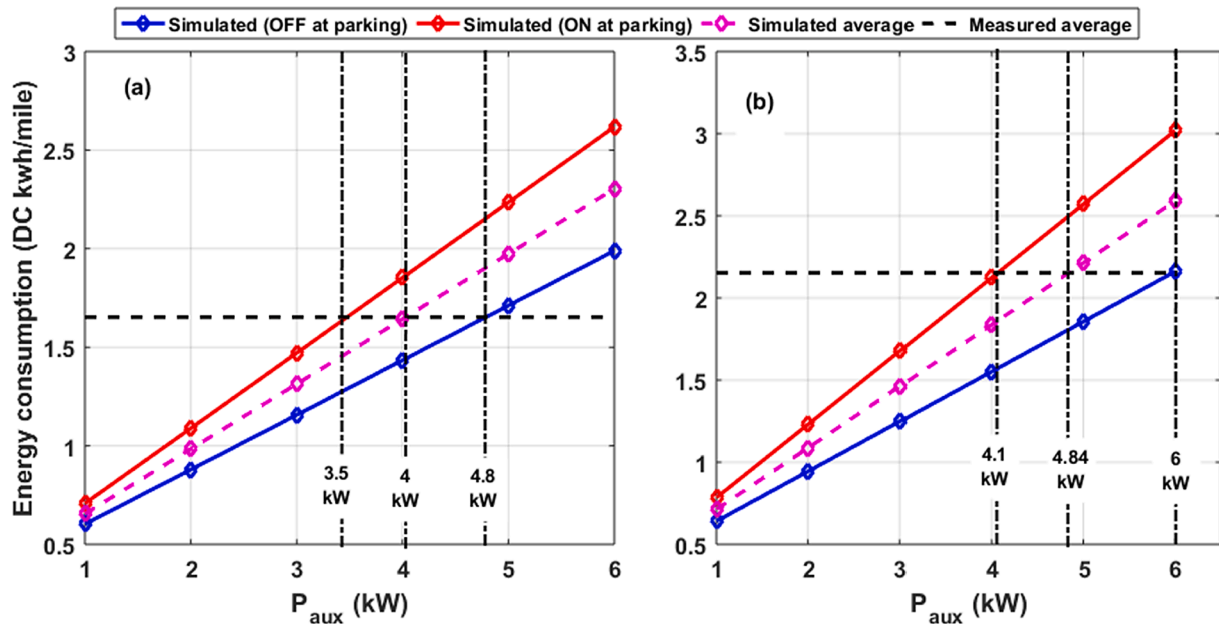


Fig. 3. Energy consumption vs. auxiliary loads. (a) Arma1. (b) Arma2.

A_f is the frontal area (m^2), $v(\tau)$ is the driving speed at the current time step (τ) (m/s), $v(\tau - 1)$ is the speed at the prior time step ($\tau - 1$), G is gravity (9.8 m/sec^2), and g is the road grade (%). M_v is the total vehicle mass (kg), which is modeled as a function of the base mass for the vehicle without the battery (M_{base}) and the battery density D_b (kWh/kg), as presented in Eq. (5). The Arma shuttle parameters considered for the model are indicated in Table 2 [33].

$$M_v = M_{base} + D_b \times Q_b \quad (5)$$

3.2. Auxiliary loads estimation

The power due to auxiliary loads of Arma shuttles is analyzed considering the measured data in Fig. 2 and Table 1. Speed profiles are fed to the powertrain model, and the energy consumption (DC kWh/mile) is estimated considering different values of P_{aux} . The estimated DC kWh/mile are compared with the average measured value for the three-day data assuming a 90% plugin charger efficiency. Two assumptions are analyzed: (a) vehicle was on during parking (provides a minimum estimation of P_{aux}), and (b) vehicle was off during parking (provides a maximum estimation of P_{aux}). The outcomes from this analysis are presented in Fig. 3. For Arma1 (Fig. 3[a]), P_{aux} ranges from 3.5 kW to 4.8 kW with an average of 4 kW. Arma2 (Fig. 3[b]) shows a higher range of 4.1–6 kW with an average of 4.38 kW.

The impact of charger efficiency on P_{aux} estimation is explored in Table 3. Assuming higher charger efficiency leads to higher estimation for P_{aux} . While present-day automated systems show relatively high-power demands for the accessory loads (3.5–6 kW), it is expected to see lower values in future scenarios with computing advancements and efficiency improvements. The average values at 90% charger efficiency (4 kW for Arma1 and 4.84 kW for Arma2) are considered for modeling

the present-day vehicle operation, while expected future operation values of 1.4 and 1.7 kW are considered for Arma1 and Arma2, respectively [34].

3.3. In-Route inductive charger power model

In inductive charging system, the electric power transfers from a stationary transmitter coil in the road to a mobile receiver coil in the vehicle by electromagnetic coupling. The power model of an in-route inductive charger presented in [4] is considered for this work. The coil consists of 5-meter segments that are stacked together to form a transmitter coil with a specific length. The power profile of each segment shows a trapezoidal shape in the travel direction and a parabolic shape in the lane direction, as indicated in Fig. 4 [29,35]. This profile is implemented as a look up table with the ability to adjust the maximum power and number of segments.

The potential locations of inductive chargers are predefined to cover most of the travel route. A total of 12 positions are identified, as marked in Fig. 1. The first two positions (red) match with the north and south stops, and are defined as quasi-dynamic, since the charging will happen during transient stops and slow travel. The remaining positions (purple) are located on the road and are defined as dynamic, since the charging will occur while the vehicle is moving. The structure and operation of the inductive transmitters at all positions are identical. A charging event starts and continues as long as the vehicle pad is fully or partially aligned with a transmitter segment. The charging time depends on the vehicle speed (fully stop, moving slowly, or moving at high speed). The proper number and locations of inductive chargers (N_{IPT}), the number of track segments at each position (N_s), and the charging power level (P_c) are optimized to realize the balance between the overall system cost and performance.

Table 3
Auxiliary loads estimation assuming different charger efficiencies.

Plugin charger efficiency	Load of Arma1 (kW)			Load of Arma2 (kW)		
	Minimum	Maximum	Average	Minimum	Maximum	Average
85%	3.24	4.46	3.75	3.8	5.58	4.52
90%	3.5	4.8	4	4.1	6	4.84
95%	3.72	5.12	4.31	4.33	6.33	5.16

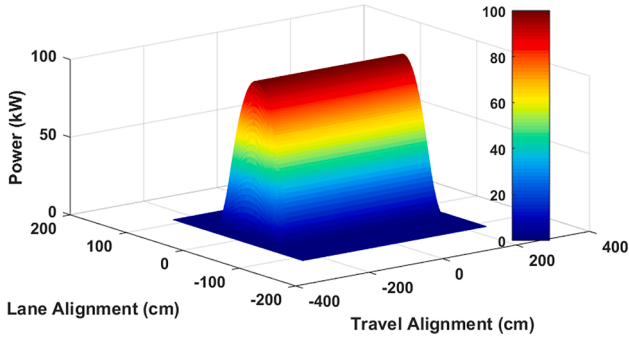


Fig. 4. Power transfer profile for a 100-kW, 5-m inductive transmitter, considering vehicle's position in both travel and lane directions.

3.4. Planning tool of inductively charged SAEV system

The vehicle's powertrain model in Sections 2.1 and 2.2 is integrated with the inductive charger power model in Section 2.3 to form an energy estimation layer in the planning tool. This layer receives real-world GPS travel data of Navya shuttles (driving speed and route) and estimates the battery power (P_{bat}), energy, and SOC profiles for a given vehicle and charger characteristics, as indicated in Fig. 5. P_{bat} is estimated based on the location of the vehicle with respect to inductive chargers and whether it is running over an IPT segment or not, as presented in Eq. (6).

$$P_{bat}(\tau) = \begin{cases} P_E(\tau) & \text{vehicle runs over a nonelectrified segment} \\ P_E(\tau) - P_{IPT}(\tau) & \text{vehicle runs over an IPT segment} \\ P_{max} & \text{vehicle is parked and turned on} \\ 0 & \text{vehicle is parked and turned off} \end{cases} \quad (6)$$

Another optimization layer is linked to the energy estimation layer, which includes an automatic search algorithm and cost models for the charging infrastructure and battery. The search algorithm receives energy and SOC profiles, evaluates predefined objectives and constraints, and updates the input parameters (for charger and vehicle) to minimize the overall system cost, while satisfying the given constraints.

4. System planning problem formulation

SAEV service supported by in-route inductive chargers experiences a trade-off between the vehicle's driving range and overall system cost. Deploying redundant infrastructure can provide a significant extension to the driving range (specifically to infinity), however it may result in a very expensive system. Therefore, there is a need to optimize the system

characteristics to realize a target driving performance at minimum cost. A nonlinear mixed-integer (NLMI) optimization problem is formulated and solved to find the best combination of the system key design parameters that achieves an optimum balance between cost and performance.

4.1. Optimization variables

The cost and performance of an inductively charged SAEV system are extensively impacted by four main variables: (1) number and locations of inductive chargers ($x_1 = N_{IPT}$), (2) charger maximum power ($x_2 = P_c$), (3) number of inductive segments at each position ($x_3 = N_s$), and (4) onboard battery capacity ($x_4 = Q_b$). N_{IPT} , P_c , and N_s directly impact the IPT system cost, while Q_b and P_c influence the vehicle cost. The coupling among these variables is considered within the optimization objective, represented by the overall system cost, and constraints that are evaluated using the vehicle powertrain and inductive charger power models. Optimizing these variables will help balancing the cost increase due to the IPT system infrastructure with the decrease in vehicle cost due to battery reduction.

4.2. Cost models

Cost models for the SAEV system, considering different charging technologies (in-route inductive chargers, DCFCs, and L2 chargers) are developed for optimization purposes.

4.2.1. Cost model of SAEV with in-route inductive chargers

A cost model for inductively charged SAEV system is developed to include the unit and installation costs for both the road and vehicle components. The road components cost ($C_{r,IPT}$) includes road retrofitting, power converters, control, materials, grid connectivity, and installation costs. This cost is a function of number, locations, length, and nominal power of inductive charger, as presented in Eq. (7).

$$C_{r,IPT}(x) = N_L L_s x_1 x_3 (c_r + c_{em} x_2 + c_g x_2) + c_{i,IPT} x_1 \quad (7)$$

where x denotes an optimization variable (x_1 – x_4); L_s is the inductive segment length (miles); N_L is the number of electrified lanes per road; c_r is the road construction cost coefficient (\$/[mile.lane]); c_{em} is the road electronics and materials cost coefficient (\$/[mile.kW.lane]); c_g is the grid connectivity cost coefficient (\$/[mile.kW.lane]); and $c_{i,IPT}$ is the transmitter installation cost coefficient (\$/position).

The other cost component is related to the vehicle ($C_{v,IPT}$), which comprises the onboard battery and inductive vehicle assembly costs, as

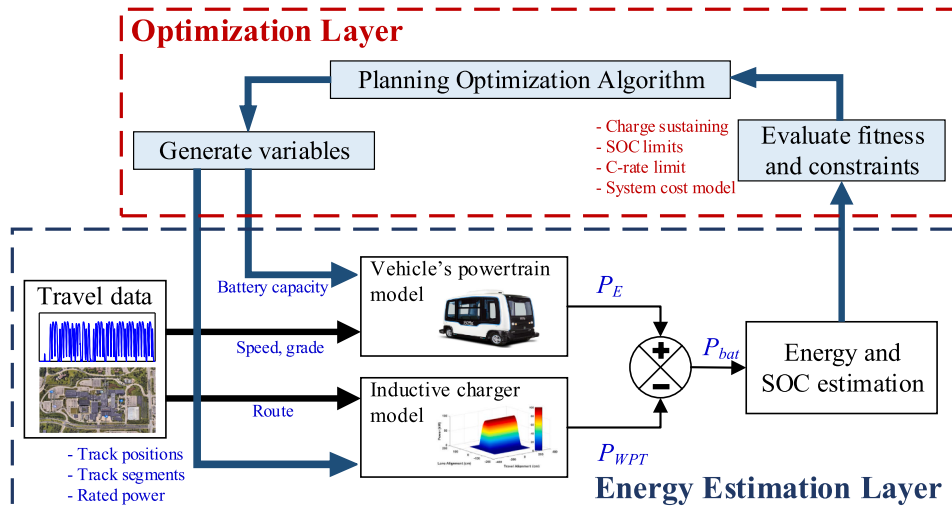


Fig. 5. System planning and optimization tool.

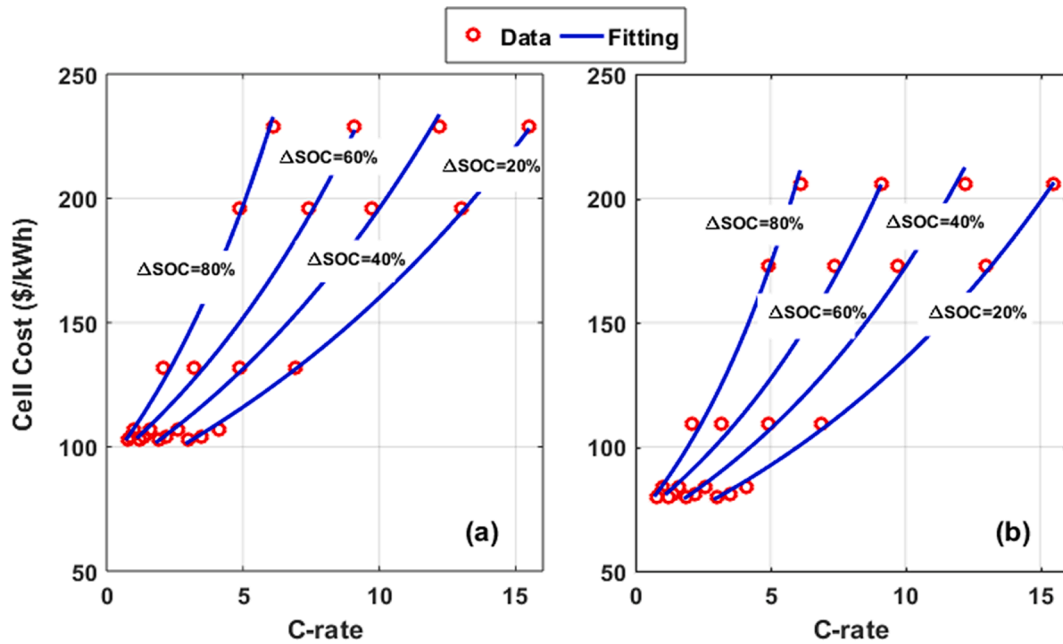


Fig. 6. Battery cell cost coefficient as a function of C-rate capability and ΔSOC window. (a) Present-day. (b) Future.

Table 4
Battery cost coefficients for present-day and future scenarios.

ΔSOC	Future	Present
20%	$a = 63.152, b = 0.0764$	$a = 84.05, b = 0.0644$
40%	$a = 66.66, b = 0.095$	$a = 87.982, b = 0.0801$
60%	$a = 71.001, b = 0.1168$	$a = 92.751, b = 0.0986$
80%	$a = 70.555, b = 0.1798$	$a = 92.284, b = 0.1517$

formulated in Eq. (8). The overall system cost is the summation of these two cost components.

$$C_{v_IPT}(x) = N_{SAEV}(c_b x_4 + c_{VA} N_{pad} x_2) \quad (8)$$

where N_{pad} is the number of inductive pads per vehicle; N_{SAEV} is the number of SAEVs to be supported by IPT system; c_{VA} is the vehicle assembly cost coefficient (\$/kW); and c_b is the onboard battery module cost coefficient (\$/kWh).

4.2.2. Cost model of SAEV with DCFCs

For DCFCs, the vehicle does not carry any electronic components onboard. Therefore, a cost model for SAEV system supported with DCFCs is formulated to include the unit and installation costs of EVSE and onboard battery cost, as indicated in Eq. (9):

$$C_{L_DCFC} = N_{DCFC} P_c [c_{DCFC} + c_{DCFC_i}] + N_{EV} c_b Q_b \quad (9)$$

where N_{DCFC} is the number of charging ports, c_{DCFC} is the DCFC unit cost coefficient (\$/kW), and c_{DCFC_i} is the installation cost coefficient (\$/[kW.port]).

4.2.3. M. Cost model of SAEV with L2 AC chargers

Vehicles support L2 AC charger will carry onboard electronics that convert the input AC power to DC to supply its battery. A cost model for SAEV system supported by L2 chargers incorporates the unit and installation costs of EVSE, onboard battery, and onboard charger, as described in Equation (10):

$$C_{L_L2} = N_{L2} [c_{L2} P_c + c_{L2_i}] + N_{EV} [c_b Q_b + c_{OBC} P_c] \quad (10)$$

where N_{L2} is the number of charging ports, c_{L2} is the L2 charger unit cost coefficient (\$/kW), c_{L2_i} is the installation cost coefficient (\$/port), and c_{OBC} is the onboard charger cost coefficient (\$/kW).

4.2.4. N. Battery cell cost estimation

The battery cost coefficient (c_b) varies with the battery cell charging rate (C-rate) capability and the actual operating SOC window (ΔSOC), as reported in [36]. For the same operating window, c_b increases as increasing the C-rate capability because higher C-rate capability involves thinner cell electrodes. For the same C-rate capability, c_b decreases as decreasing the operating window. Considering the NMC622-Graphite, 85-kWh, 900 DCV battery pack, the variation of c_b with respect to C-rate and ΔSOC is described in Fig. 6(a) [36]. In this case, a cost of \$103/kWh for 1C and 80% ΔSOC is considered, which reflects present-day battery costs. However, for future assumptions, the U.S. Department of Energy (DOE) Vehicles Technologies Office (VTO) 2015 target for a battery cell cost, \$80/kWh, is considered for 1C and 80% ΔSOC, as indicated in Fig. 6(b) [36]. The data points provided in [36] and shown in red circles are curve fitted to produce the generic mathematical model described in Eq. (11). This model represents the nonlinear relationship between c_b and C-rate at a certain ΔSOC. The coefficients of this model (a and b) vary for different ΔSOC, as presented in Table 4 for both present-day and future scenarios.

$$c_b = a \cdot e^{b \cdot C_rate} \quad (11)$$

Table 5
Settings of two operating scenarios: present-day and future.

Coefficient	Future	Present
Driving range for over-night	12 h	12 h
Auxiliary loads (kW)	1.4 & 1.7	4 & 4.38
c_r (M\$/[mile.lane])	1	1.2
c_e (M\$/[mile.kW.lane])	0.0273	0.033
c_g (M\$/[mile.kW.lane])	0.015	0.018
c_{IPT} (M\$/position)	0.005	0.005
c_{VA} (\$/kW)	29	66.67
c_b (\$/kWh) @ 1C and 80% ΔSOC	80	103
c_{DCFC} unit cost (\$/kW)	300	600
c_{DCFC_i} (\$/[kW.port])	400	400
c_{L2} unit cost (\$/kW)	125	250
c_{L2_i} (\$/port)	2500	2500
c_{OBC} (\$/kW)	50	100

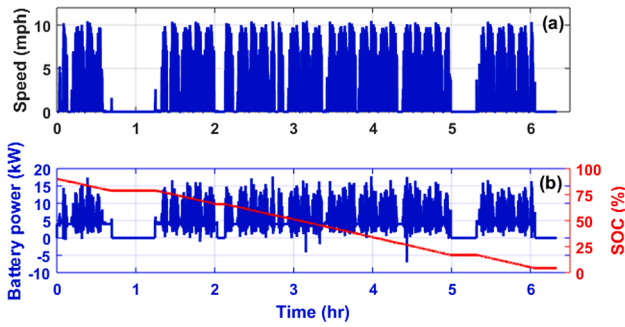


Fig. 7. Current driving performance of Arma1 on July 19, 2018. (a) Real-world speed profile. (b) Simulated battery power and SOC profile.

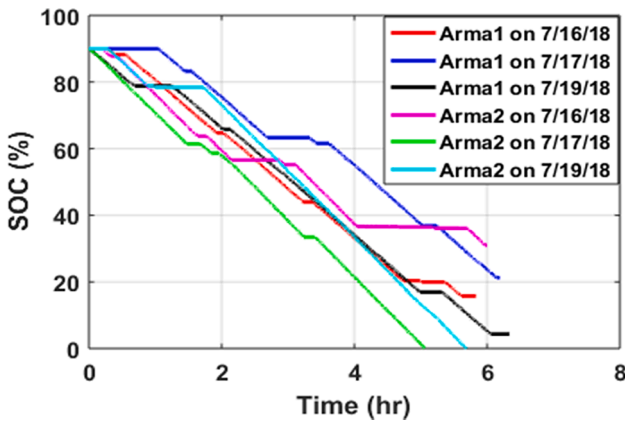


Fig. 8. Current driving performance (SOC profiles) of Arma1 and Arma2 in July 16, 17, and 19, 2018.

4.3. Optimization constraints

Planning optimization problem of an inductively supported SAEV system entails constraints related to the vehicle driving performance, battery performance, and boundaries of optimization variables, as stated in (12). C_1 is an inequality constraint that guarantees charge-sustaining operation by limiting the difference between the final (SOC_f) and initial SOC (SOC_i) to be less than a predefined small value (ϵ). C_2 – C_4 is a set of inequality constraints that limit the battery charging and discharging process to avoid overcharging, deep discharging, and high C-rate. C_5 is a set of bound constraints that defines the lower and upper limits of optimization variables. C_6 is a set of integer variable constraints that forces optimization variables to be integer. These constraints are considered for limiting the search space for the optimum solution.

$$\begin{aligned}
 C_1 : \text{charge - sustaining operation} : & \quad |SOC_f - SOC_i| \leq \epsilon\% \\
 C_2 : \text{acceptable minimum SOC limit} : & \quad SOC_{min} \geq A\% \\
 C_3 : \text{acceptable maximum SOC limit} : & \quad SOC_{max} \leq B\% \\
 C_4 : \text{acceptable maximum battery C - rate} : & \quad C_{rate} \leq C_{r,lim} \\
 C_5 : \text{boundaries} : & \quad x_k^L \leq x_k \leq x_k^U \quad \forall k = 1, 2, 3, 4 \\
 C_6 : \text{integer variables} : & \quad x_k > 0, x_k \in Z^+ \quad \forall k = 1, 2, 3, 4
 \end{aligned} \tag{12}$$

5. Results and discussion

The planning optimization platform was implemented and solved in a MATLAB environment. A single-objective system design optimization problem is analyzed using a NLMI solver based on genetic algorithm (GA). The optimum system design is evaluated for all SAEVs at the Navya shuttle project. Two operating scenarios are investigated:

Table 6
Ranges of search variables for each optimization run.

Variable	QDIPT1	QDIPT2	DIPT
$x_1 = N_{IPT}$	{1, 2, 3}	{1, 2, 3}	[1–4095 ($2^{12}-1$)]
$x_2 = P_c$ (kW)	{10, 20, ..., 100}	{10, 20, ..., 100}	{10, 20, ..., 100}
$x_3 = N_c$	1	1	{1, 2, ..., 10}
$x_4 = Q_b$ (kWh)	{1, 2, ..., 100}	33	{1, 2, ..., 100}

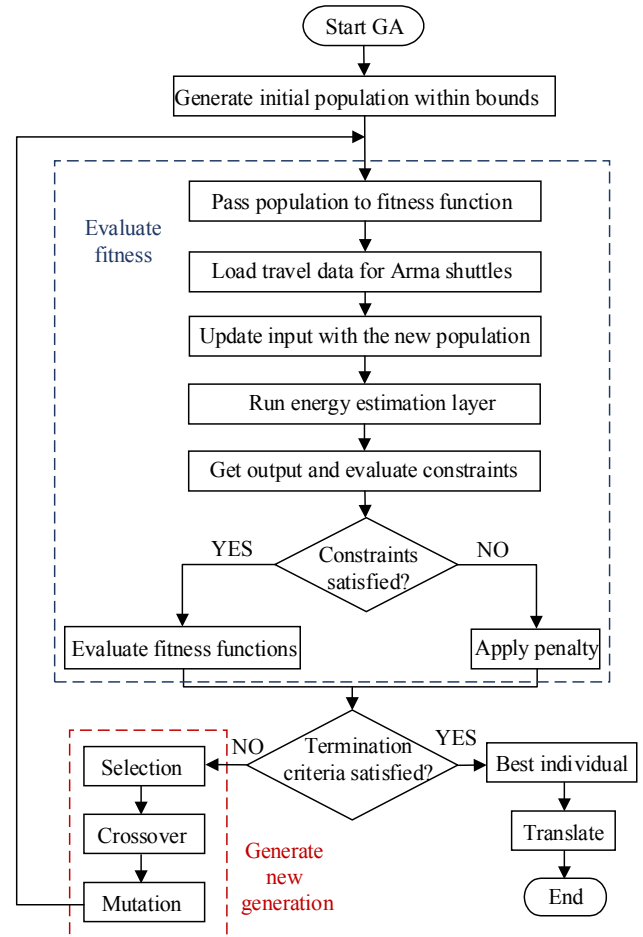


Fig. 9. Flow-chart for solving planning optimization problem using GA.

present-day and future. For both scenarios, the low-speed driving data are considered because of the need for this operation in the university campus, whether currently or in the future. The differences between the two scenarios are the vehicle’s auxiliary loads and system cost coefficients. The settings for both scenarios are listed in Table 5.

The cost factors are defined based on: (1) the U.S. DOE VTO 2015 cost target for power electronic, which declares \$12/kW [37]; (2) the current and expected future market prices for materials (ferrite, litz wires, shield, etc.) and capacitors, considering cost scaling factors for bulk purchases and gross manufacturing; (3) available data in the literature; and (4) transportation entities for construction costs. Considering both operating scenarios (present and future), four different charging and vehicle options are explored: (a) a small onboard battery with in-route quasi-dynamic inductive chargers at stops, (b) a small onboard battery with in-route dynamic and quasi-dynamic inductive chargers, (c) a large onboard battery with stationary DCFs, and (d) a large onboard battery with stationary L2 chargers.

Table 7
GA solver settings and optimization parameters.

Parameter	Value	Parameter	Value
Populations	20	N_{pad}	1
Mutation	Uniform 0.02	L_s	5 m
Crossover	0.7	A	40%
Generations	50	B	99%
Runs	2	ϵ	10%
Penalty	200	SOC_i	90%
N_{SAEV}	2	$C_{r,lim}$	4C

5.1. Current performance of Arma SAEVs

The current driving performance of Navya SAEVs is evaluated using the developed platform and driving data from Section 2.2. In this case, each shuttle is supported with a 33-kWh onboard battery and runs without in-route charging capability. The driving performance of Arma1 on July 19, 2018 is simulated and presented in Fig. 7. As the figure demonstrates, a full battery charge allows the shuttle to run for about 6.5 h with long intermittent stops (about 5 h continuous operation). The SOC profiles of the two vehicles considering the three days of driving data are shown in Fig. 8, which shows a range of 5–6.5 h of total operating hours. Therefore, to extend the vehicles range to 12 h without stopping for plug-in and interrupting the service, in-route automatic inductive charging capability is needed—either dynamic or quasi-dynamic.

5.2. In-route inductive charging system

Several NLMI single-objective planning optimization problems for SAEV supported by in-route inductive charging are formulated and analyzed, considering different potential charging positions (at stops and/or on the road) and operating scenarios (present and future):

5.2.1. S. Quasi-dynamic IPT (QDIPT) charging with optimum onboard battery (QDIPT1)

In this case, inductive chargers are allocated at designated stops only (red segments in Fig. 1) for quasi-dynamic charging. Therefore, only three options for the allocation are considered: at north stop only, at south stop only, or at both. A fixed, single segment of primary coil is assumed at each position. In this case, three search variables are optimized: N_{IPT} , P_c , and Q_b , as indicated in Table 6. N_{IPT} defines the locations of chargers and ranges from 1 to $2^{12}-1$ (4095) due to the availability of 12 locations. $N_{IPT} = 1$ (10000000000) means that there is a charger at the first position only. $N_{IPT} = 3$ (110000000000), means that there are chargers at the first and second positions.

5.2.2. T. QDIPT charging with the current SAEV (QDIPT2)

In this case, the current installed battery is kept fixed (33 kWh) and only two variables are optimized: N_{IPT} and P_c .

5.2.3. U. Dynamic IPT charging (DIPT)

In this case, both quasi-dynamic and dynamic positions (red and purple segments in Fig. 1 for inductive chargers are considered and four variables are optimized: N_{IPT} , N_s , P_c , and Q_b . The ranges for the search variables considered at each optimization are indicated in Table 6.

To minimize the computational time involved with the optimization, one day of data for each SAEV was considered. These days are chosen to represent the worst operation for each vehicle that show the least driving range and the largest energy consumption. July 19 was chosen for Arma1 and July 17 represented Arma2 (see Fig. 8). The above-mentioned optimization problems are solved using GA, which is a stochastic search approach that emulates biological evolutionary theory to solve nonlinear optimization problems [38]. GA is linked to the planning tool to solve the NLMI optimization problem based on the follow-chart in Fig. 9. The settings of GA solver are presented in Table 7. Each

Table 8
Optimization results for in-route inductive charging, considering different operating scenarios.

Technology	Present				Future		
	QDIPT1		QDIPT2		QDIPT1		DIPT
	S1	S2	S1	S1	S1	S2	S1
Solution							
# chargers	2	1	1	1	1	1	1
Location	S & N	N	N	N	N	N	N
P_c (kW)	50	100	100	100	40	50	40
N_s	1	1	1	1	1	1	1
Q_b (kWh)	29	28	33	28	29	14	29
C-rate	1.55	3.2	2.73	3.2	1.24	3.2	1.24
kWh/mile	1.647	1.647	1.649	1.647	0.792	0.785	0.792

optimization runs twice, and each run involves testing of 1000 chromosomes (20 populations times 50 generations). Because of the integer nature of optimization variables, a uniform mutation is chosen with a rate of 2%, which means that a consistent 2% of genes is selected to be mutated and set to random values between the user-specified upper and lower bounds for that gene. A crossover rate of 70% is chosen, which defines the probability that two chromosomes may swap their bits. These values are decided by trial and error to show a good optimization performance by realizing the least fitness function as quick as possible. The optimization parameters are indicated in Table 7 based on assumptions below:

- Each SAEV carries a single inductive pad ($N_{pad} = 1$).
- Each segment of inductive charger is 5-m long ($L_s = 5$ m).
- The initial, minimum, and maximum allowed SOC are 90%, 40%, and 99%, respectively.
- The maximum operating SOC window for charge-sustaining operation (ϵ) is 10%.
- The maximum limit for C-rate ($C_{r,lim}$) is 4C [39].

The DIPT and QDIPT optimization results considering present and future scenarios are presented in Table 8. The optimization results show that high-power chargers present the most cost-effective overall system due to the associated smaller number of chargers and coil length and road construction work, which is the dominant cost component of an in-route inductive charger. The outcomes show that for present-day scenarios, charge-sustaining operation is realized by installing 50-kW quasi-dynamic inductive chargers at the designated stops N and S with one five-meter segment per position and a 29-kWh onboard battery (QDIPT1, S1). Another optimal solution (QDIPT1, S2) shows that a single 100-kW quasi-dynamic inductive charger at the north stop with one segment per position and a 28-kWh onboard battery allows the vehicles to realize charge-sustaining operation and presents the least overall system cost. This solution is valid even if the current vehicles with 33-kWh batteries are considered, as proved in QDIPT2, S1. Solving for DIPT while considering all the road segments (red and purple in Fig. 1) outputs the same solutions as the quasi-dynamic scenario, which makes perfect sense for realizing the global optimum solution that shows a minimum overall system cost. Solutions for future scenarios require less charging power and smaller batteries because of the higher vehicle efficiency. In these scenarios, charge-sustaining operation was realized using either one 40-kW charger at the north stop with a 29-kWh battery or one 50-kW charger at the north stop with a 14-kWh battery.

As an example, the driving performance of Arma1 on July 19 considering QDIPT1, S2 optimal solution is indicated in Fig. 10. The figure shows SOC and battery power profiles over time. As noted, each time the vehicle passes through the inductive charger at the north stop, it receives about 100 kW inductive power. This allows the vehicle to realize charge-sustaining operation showing a near-flat SOC profile, compared to the decaying profile in Fig. 7. This performance has the potential to allow the vehicle to run continuously without the need to

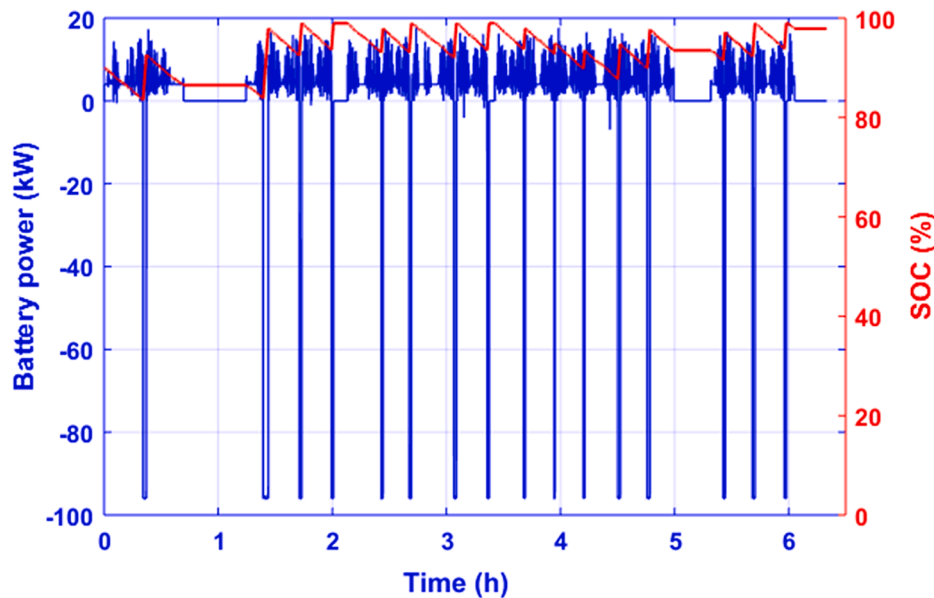


Fig. 10. SOC and battery power profile of Arma1 on July 19, considering QDIPT1, S2 for present-day scenario.

Table 9
Results for overnight charging, considering different operating scenarios.

Technology	Present		Future	
	DCFC	L2 charger	DCFC	L2 charger
# chargers	1	2	1	2
Location	Garage	Garage	Garage	Garage
P_c (kW)	252	7.9	109	3.4
Q_b (kWh)	70.1	70.1	30.2	30.2
T_c	15 min	8 h	15 min	8 h
C-rate	3.24	0.1	3.24	0.1
kWh/mile	1.98	1.98	0.79	0.79

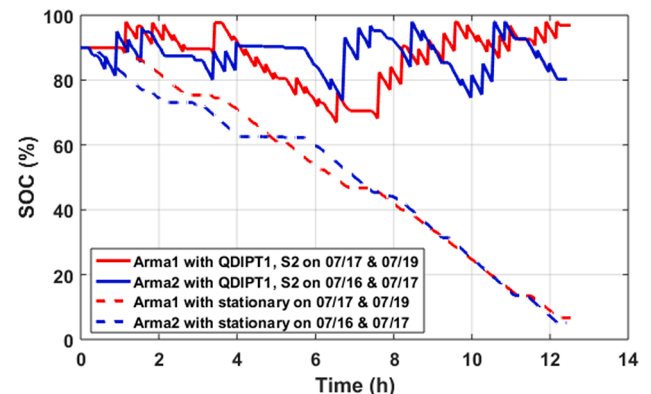


Fig. 12. SAEV performance, considering different charging technologies for future operation.

5.3. Overnight stationary conductive charging

Performance and feasibility of stationary conductive charging technologies (DCFCs and L2 chargers) are explored for the Navya shuttles. In this case, the vehicle is supported by a large onboard battery to fulfill a target driving range of 12 h and a stationary conductive charger is installed at the garage area for overnight charging to fully charge the battery within a target charging time, $T_c = 15$ min, according to the DOE VTO target [36]. However, the L2 chargers are set to a target of 8 h to represent the overnight period. Parameters in Table 5 are considered for deciding the battery capacity, charger nominal power, and overall system cost.

The results of overnight conductive charging analysis are presented in Table 9. As noted, continuous driving for 12 h in present-day technology requires about 70.1-kWh onboard battery, while a future scenario needs 30.2-kWh battery size. This is because of the inefficient operation of present-day SAEVs. In addition, a 252-kW (for present-day) or 109-kW (for future) DCFC is needed to fully charge the batteries of both shuttles within 30 min (15 min for each SAEV). On the other hand, two 7.9-kW (for present-day) or two 3.4-kW (for future) L2 chargers are required to fully recharge the batteries of two shuttles within 8 h.

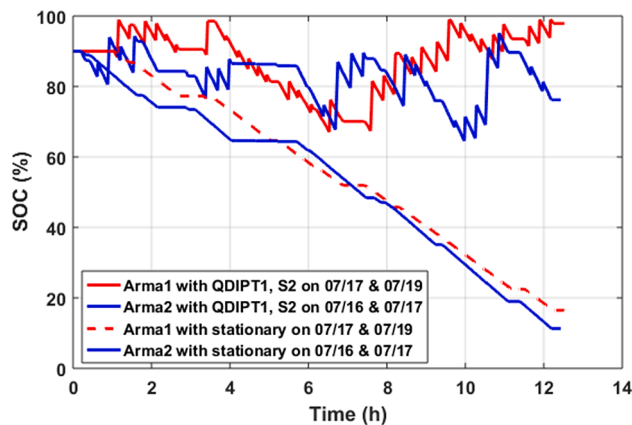


Fig. 11. SAEV performance, considering different charging technologies for present-day operation.

stop for recharging. With around 100-kW charger power spikes, vehicle battery realizes C-rates of less than 4C, which is defined by constraint C_4 in equation (12) and Table 7. This limit was chosen based on [39], which shows up to 6C continuous charging for 800 cycles with just 10% capacity loss [39]. For a pulse charging profile within a narrow SOC window, shown in Fig. 10, these cells can presumably tolerate even more cycles. Therefore, 4C presents a reasonable C-rate limit a such application.

Table 10
Techno-economic comparison among QDIPT, DCFCs and L2 charger.

Characteristic	QDIPT	DCFC	L2 charger
Driving range	Unlimited	Limited (12 h)	Limited (12 h)
Recharge time	Zero	30 min	8 h
Vehicle components cost	Medium+	High	Medium
Road components cost	Medium	High	Low
Overall system cost	Medium+	Very high	Medium
Service interruption	Low	Medium	High
Land requirement	Low	High	
Energy consumption	Low	High	
Automatic	Yes	No	
User discomfort	Low	High (plug-in)	
Hazards	Electromagnetic fields	Mechanical connection, arcing, exposed conductor, etc.	
Visual pollution	Low	High	

5.4. Techno-economic comparative analysis

The optimum solution (QDIPT1, S2) for in-route inductive charging, along with the results of stationary charging, are inserted to the vehicle and charger models to evaluate their impact on the vehicle driving performance. The SAEV performance considering present and future operations are indicated in Figs. 11 and 12, respectively. The figures show that using in-route inductive charging (one segment of 100-kW QDIPT system for present-day or 50-kW for future at the north stop with a 28-kWh battery for present-day or 14-kWh for future) allows the vehicles to realize charge-sustaining operation (unlimited driving range and zero recharge downtime) showing near-flat SOC profiles. Additionally, all SAEVs operates with in a narrow SOC operating window, which helps to improve battery performance and life. On the other hand, installing large onboard batteries on the vehicles (70.1-kWh for present-day and 30.2-kWh for future) along with stationary overnight charging (DCFCs and L2) show a limited driving range of ~12 h, after which the vehicles must stop for recharging. Compared to the current installed battery, in-route inductive charging can reduce the required battery capacity by about 15%, while enabling unlimited range, but stationary scenarios require about 112% additional battery capacity to support a 12 h driving range.

By comparing the costs of in-route inductive charging and overnight charging, the outcomes show that DCFC solution shows the highest overall system cost because of: (1) the high vehicle component cost associated with large onboard battery and high C-rate, and (2) high rating and cost of EVSEs. QDIPT solutions are much more cost-effective compared to DCFC due to the lower vehicle components and EVSE cost. L2 chargers with an 8-h charging time is the most cost-effective solution, however, they are not appropriate for automated vehicles because they are not automatic, there is a high risk to interrupt service, they provide a limited range, and the vehicle has high energy consumption and operating costs, as described in Table 10. Beside that, in-route chargers are easier to use, safer, and do not need designated land because they will be installed on the road at stops.

6. Conclusion

This study presents system design and feasibility analyses of in-route inductive charging for fixed-route circulator SAEVs compared to stationary conductive charging technologies. The key findings are summarized as follows:

- Implementing in-route inductive charging technology for SAEVs is an appropriate solution for realizing a fully automated mobility system (both vehicle and charger)
- For low-speed (10–15 mph) SAEV operation (e.g., university campuses, airports, research facilities), considering present-day costs and

vehicles, the charge-sustaining operation is realized by implementing 50-kW quasi-dynamic inductive chargers at the designated stops with one 5-m segment per position and a 29-kWh onboard battery

- Another optimal solution shows that only one 100-kW quasi-dynamic inductive charger at the north stop with one segment per position and a 28-kWh onboard battery allows the vehicles to realize charge-sustaining operation and shows the minimum-cost solution when considering the cost parameters defined in Table 5.
- Considering future costs and vehicles, the charge-sustaining operation was realized using either one 40-kW charger at the north stop with a 29-kWh battery or one 50-kW charger at the north stop with a 14-kWh battery.
- DCFCs solution shows the highest vehicle components cost, EVSEs cost, and overall system cost.
- Quasi-dynamic inductive solutions are much more cost-competitive compared to stationary fast charging, and more convenient for automated vehicles than L2 chargers.
- Quasi-dynamic inductive solution can reduce the onboard battery by about 15% while providing unlimited driving range, but stationary scenarios require about 112% additional battery capacity to support a 12-h driving range.

CRediT authorship contribution statement

Ahmed A.S. Mohamed: Conceptualization, Methodology, Software, Writing - review & editing. **Eric Wood:** Methodology, Visualization, Investigation, Writing - review & editing. **Andrew Meintz:** Conceptualization, Supervision, Investigation.

Declaration of Competing Interest

The authors declare that they have no known competing financial interests or personal relationships that could have appeared to influence the work reported in this paper.

Acknowledgment

This work was authored by the National Renewable Energy Laboratory (NREL), operated by Alliance for Sustainable Energy, LLC, for the U.S. Department of Energy (DOE) under Contract No. DE-AC36-08GO28308. Funding provided by the U.S. Department of Energy Office of Energy Efficiency and Renewable Energy Vehicles Technologies Office (VTO) under the Systems and Modeling for Accelerated Research in Transportation (SMART) Mobility Laboratory Consortium, an initiative of the Energy Efficient Mobility Systems (EEMS) Program. The authors acknowledge John Smart of INL for leading the Alternative Fuel Infrastructure Pillar of the SMART Mobility Laboratory Consortium. The following DOE Office of Energy Efficiency and Renewable Energy (EERE) managers played important roles in establishing the project concept, advancing implementation, and providing ongoing guidance: David Anderson, and Erin Boyd. The views expressed in the article do not necessarily represent the views of the DOE or the U.S. Government. The U.S. Government retains and the publisher, by accepting the article for publication, acknowledges that the U.S. Government retains a nonexclusive, paid-up, irrevocable, worldwide license to publish or reproduce the published form of this work, or allow others to do so, for U.S. Government purposes.

References

- [1] Transportation Research Board. Critical Issues in Transportation, The National Academies of Sciences, Engineering and Medicine; 2013. Available: <http://www.trb.org/Publications/Blurbs/169945.aspx>.
- [2] Sun L, Wang S, Liu S, Yao L, Luo W, Shukla A. A complete research on the feasibility and adaptation of shared transportation in mega-cities – a case study in Beijing. *Appl Energy* 2018;230:1014–33. <https://doi.org/10.1016/j.apenergy.2018.09.080>.

- [3] Fulton L, Mason J, Meroux D. Three revolutions in urban transportation, ITDP, UC Davis, Academic Research, May 2017. Available: <https://www.itdp.org/publication/3rs-in-urban-transport/>.
- [4] Mohamed AAS, Meintz A, Zhu L. System design and optimization of in-route wireless charging infrastructure for shared automated electric vehicles. *IEEE Access* 2019;7:79968–79. <https://doi.org/10.1109/ACCESS.2019.2920232>.
- [5] Hu Y, Zhang Y, Lamb D, Zhang M, Jia P. Examining and optimizing the BCycle bike-sharing system – a pilot study in Colorado, US. *Appl Energy* 2019;247:1–12. <https://doi.org/10.1016/j.apenergy.2019.04.007>.
- [6] Baxter JA, Merced DA, Costinett DJ, Tolbert LM, Ozpineci B. Review of electrical architectures and power requirements for automated vehicles. In: 2018 IEEE Transportation Electrification Conference and Expo (ITEC); 2018. p. 944–9. <https://doi.org/10.1109/ITEC.2018.8449961>.
- [7] Luo L, et al. Optimal planning of electric vehicle charging stations comprising multi-types of charging facilities. *Appl Energy* 2018;226:1087–99. <https://doi.org/10.1016/j.apenergy.2018.06.014>.
- [8] Mohamed AAS, Shaier AA, Metwally H, Selem SI. A comprehensive overview of inductive pad in electric vehicles stationary charging. *Appl Energy* 2020;262:114584. <https://doi.org/10.1016/j.apenergy.2020.114584>.
- [9] Mohamed AAS, Zhu L, Meintz A, Wood E. Planning optimization for inductively charged on-demand automated electric shuttles project at Greenville, South Carolina. *IEEE Trans Ind Appl* 2019;1. <https://doi.org/10.1109/TIA.2019.2958566>.
- [10] Guo Y, Wang L, Zhu Q, Liao C, Li F. Switch-on modeling and analysis of dynamic wireless charging system used for electric vehicles. *IEEE Trans Ind Electron* 2016; 63(10):6568–79. <https://doi.org/10.1109/TIE.2016.2557302>.
- [11] Deng J, Pang B, Shi W, Wang Z. A new integration method with minimized extra coupling effects using inductor and capacitor series-parallel compensation for wireless EV charger. *Appl Energy* 2017;207:405–16. <https://doi.org/10.1016/j.apenergy.2017.05.088>.
- [12] Mohamed AAS, Shaier AA, Metwally H, Selem SI. Interoperability of the universal WPT3 transmitter with different receivers for electric vehicle inductive charger. *eTransportation*; 2020: 100084. doi: 10.1016/j.etrans.2020.100084.
- [13] Inductive Power Transfer for Automotive Applications: State-of-the-Art and Future Trends – IEEE Journals & Magazine. <https://ieeexplore.ieee.org/document/8359259> [accessed Mar. 06, 2019].
- [14] Shin J, et al. Design and implementation of shaped magnetic-resonance-based wireless power transfer system for roadway-powered moving electric vehicles. *IEEE Trans Ind Electron* 2014;61(3):1179–92. <https://doi.org/10.1109/TIE.2013.2258294>.
- [15] Buja G, Bertoluzzo M, Dashora HK. Lumped track layout design for dynamic wireless charging of electric vehicles. *IEEE Trans Ind Electron* 2016;63(10): 6631–40. <https://doi.org/10.1109/TIE.2016.2538738>.
- [16] Dai X, Jiang J-C, Wu J-Q. Charging area determining and power enhancement method for multiexcitation unit configuration of wirelessly dynamic charging EV system. *IEEE Trans Ind Electron* 2019;66(5):4086–96. <https://doi.org/10.1109/TIE.2018.2860537>.
- [17] Zhu Q, Wang L, Guo Y, Liao C, Li F. Applying LCC compensation network to dynamic wireless EV charging system. *IEEE Trans Ind Electron* 2016;63(10): 6557–67. <https://doi.org/10.1109/TIE.2016.2529561>.
- [18] Villa JL, Sallán J, Llombart A, Sanz JF. Design of a high frequency Inductively Coupled Power Transfer system for electric vehicle battery charge. *Appl Energy* 2009;86(3):355–63. <https://doi.org/10.1016/j.apenergy.2008.05.009>.
- [19] Mohamed AAS, Berzoy A, Mohammed OA. Physics-based FE model and analytical verification of bi-directional inductive wireless power transfer system. In: 2016 IEEE/ACES International Conference on Wireless Information Technology and Systems (ICWITS) and Applied Computational Electromagnetics (ACES), Mar. 2016. p. 1–2, doi: 10.1109/ROPACES.2016.7465447.
- [20] Mohamed AAS, Meintz A, Schrafel P, Calabro A. Testing and assessment of EMFs and touch currents from 25-kW IPT system for medium-duty EVs. *IEEE Trans Veh Technol* 2019;1. <https://doi.org/10.1109/TVT.2019.2920827>.
- [21] Calabro A, Cohen B, Daga A, Miller J, McMahon F. Performance of 200-kW inductive charging system for range extension of electric transit buses. In: 2019 IEEE Transportation Electrification Conference and Expo (ITEC); 2019. p. 1–5. <https://doi.org/10.1109/ITEC.2019.8790490>.
- [22] Choi SY, Rim CT. Recent progress in developments of on-line electric vehicles. In: 2015 6th international conference on Power Electronics Systems and Applications (PESA), Hong Kong, Hong Kong, Dec. 2015. p. 1–8, doi: 10.1109/PESA.2015.7398964.
- [23] “Norway will install the world’s first wireless electric car charging stations for Oslo taxis - The Verge.” <https://www.theverge.com/2019/3/21/18276541/norway-oslo-wireless-charging-electric-taxis-car-zero-emissions-induction> [accessed Sep. 22, 2020].
- [24] B. B. CNN, Sweden opens new road that charges electric vehicles like real-life slot cars. *CNN*. <https://edition.cnn.com/2018/04/26/motorsport/sweden-electrified-road-intl-spt/index.html> [accessed Apr. 11, 2019].
- [25] Francis J. Wireless power transfer-task 26 final report, p. 75.
- [26] Planning of In-motion Electric Vehicle Charging on Freeways – IEEE Smart Grid. <https://smartgrid.ieee.org/newsletters/february-2020/planning-of-in-motion-electric-vehicle-charging-on-freeways> [accessed Sep. 22, 2020].
- [27] Jang YJ, Jeong S, Ko YD. System optimization of the On-Line Electric Vehicle operating in a closed environment. *Comput Ind Eng* 2015;80:222–35. <https://doi.org/10.1016/j.cie.2014.12.004>.
- [28] Limb B. Optimization of roadway electrification integrating wireless power transfer: technoeconomic assessment and lifecycle analysis. *Grad. Theses Diss.*, May 2017, Available: <https://digitalcommons.usu.edu/etd/5261>.
- [29] Foote A, Onar OC, Debnath S, Chinthavali M, Ozpineci B, Smith DE. Optimal sizing of a dynamic wireless power transfer system for highway applications. In: 2018 IEEE Transportation Electrification Conference and Expo (ITEC), Long Beach, CA, USA, Jun. 2018. p. 1–6. doi: 10.1109/ITEC.2018.8450095.
- [30] Mohamed AAS, Zhu L, Meintz A, Wood E. Optimum planning for inductively charged on-demand automated electric shuttles at Greenville, South Carolina. In: 2019 IEEE industry applications society annual meeting; 2019. p. 1–10. <https://doi.org/10.1109/IAS.2019.8912343>.
- [31] Mcity Driverless Shuttle, Mcity. <https://mcity.umich.edu/shuttle/> [accessed Nov. 18, 2019].
- [32] Brooker A, Gonder J, Wang L, Wood E, Lopp S, Ramroth L. FASTSim: a model to estimate vehicle efficiency, cost and performance. In: Presented at the SAE 2015 world congress & exhibition, Apr. 2015, doi: 10.4271/2015-01-0973.
- [33] Discover AUTONOM SHUTTLE | NAVYA. <https://navya.tech/en/autonom-shuttle/> [accessed Nov. 18, 2019].
- [34] Gambhira U. *Powertrain optimization of an autonomous electric vehicle*. The Ohio State University; 2018.
- [35] Bertoluzzo M, Buja G, Dashora HK. Design of DWC system track with unequal DD coil set. *IEEE Trans Transp Electrification* 2017;3(2):380–91. <https://doi.org/10.1109/TTE.2016.2646740>.
- [36] Howell D, Boyd S, Cunningham B, Gillard S, Slezak L. Enabling fast charging: a technology gap assessment. U.S. Department of Energy; Office of Energy Efficiency & Renewable Energy, Oct. 2017.
- [37] Electrical and Electronics Technical Team Roadmap. U.S. DRIVE (Driving Research and Innovation for Vehicle efficiency and Energy sustainability), Oct. 2017.
- [38] Haupt RL, Haupt SE. *Practical genetic algorithms*. 2 ed. Hoboken, NJ: Wiley-Interscience; 2004.
- [39] Ahmed S, et al. Enabling fast charging – a battery technology gap assessment. *J Power Sources* 2017;367:250–62. <https://doi.org/10.1016/j.jpowsour.2017.06.055>.